Journal Name

ARTICLE

Minimizing geminate recombination losses in small-molecule-based organic solar cells

Received 00th January 20xx,
Accepted 00th January 20xx

DOI: 10.1039/x0xx00000x

www.rsc.org/

Rafael Sandoval-Torrientes,[a] Alexey Gavrik,[b,c] Anna Isakova,[b] Abasi Abudulimu,[b] Joaquín Calbo,[d] Juan Aragó,[d] Jose Santos, *[b] Enrique Ortí,*[d] Nazario Martin,*[a] Vladimir Dyakonov,*[c] and Larry Lüer*[b]

Small-molecule-based organic solar cells (OSCs) are a recurrent alternative to polymer-based OSCs. Due to the higher purity and definition of small molecules compared to polymers, the morphological requirements can be more relaxed. Here, we present a series of novel rhodanine-based small molecule electron donors and blend them with the standard acceptor PC70BM. By performing a target analysis on femtosecond spectroscopy data, we quantify the rates of geminate charge recombination. We are able to reproduce these rates by applying the Marcus-Levich-Jortner equation, using results from quantum chemical calculations. This shows that in a series of differently substituted compounds, one can correctly predict trends in geminate recombination rates by relying only on quantities that are easy to measure (cyclic voltammetry, optical spectra) or that can be calculated by relatively inexpensive methods such as (TD)DFT. Our method should thus accelerate the search for high-performance small-molecule photovoltaic blends.

Introduction

Organic solar cells (OSCs) present specific advantages against conventional solar cells that make them apt for special applications such as building integration and indoor photovoltaics.[1-6] However, both efficiency and environmental stability in OSCs must be substantially increased to meet industry standards. In polymer-based solar cells, both efficiency and stability are limited by the need for a precisely defined nanoscale arrangement ("bulk heterojunction"), which is usually not thermodynamically stable.[7-10] In principle, these design requirements can be relaxed through the use of small molecules for both donor and acceptor phases. Recently, examples for stable and efficient all-small-molecule OSCs have been presented.[11-13] Their current-voltage characteristics suggest that small-molecule-based OSCs can indeed exhibit good charge generation and extraction properties at the same time, showing the potential of this novel strategy. For maximum exploitation of the potential of small-molecule-based solar cells, the photophysical pathways and loss channels must be understood in detail. In polymer-based solar cells, ample and detailed analyses are available in relation to morphology,[14, 15] attributing high internal quantum yields to contributions from quantum coherence[16] and delocalized states allowing long-range charge transfer, thus avoiding a strongly bound charge transfer intermediate.[17, 18]

It is important to extend these investigations to small-molecule-based OSC materials. In blends of a polyfluorene (PFO) derivative with the non-fullerene acceptor perylene, evidence for long-range transfer mechanisms were found for excitons created in both PFO and perylene phases.[19] In contrast, in a prototypical all-small-molecule blend, both neutral and charged excitations were found to be localized; the observation of high internal quantum yields was justified by predicting highly activated charge recombination (Marcus inverted region).[20] However, so far, absolute rates for geminate recombination in small-molecule-based OSC materials have not yet been measured and justified in the framework of semiclassical Marcus picture.

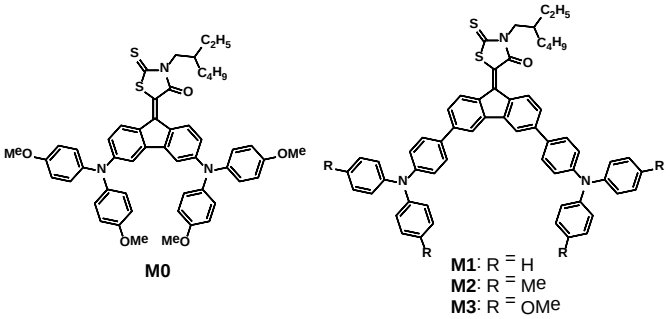

Fig. 1 Chemical structure of the donor molecules.

[a] Address Universidad Complutense de Madrid, 28040, Madrid, Spain. E-mail: nazario.martin@imdea.org
[b] Address IMDEA Nanociencia, C/ Faraday, 9, 28049 Cantoblanco, Madrid, Spain. E-mail: larry.luer@imdea.org
[c] b. Experimental Physics VI, University of Würzburg, 97074 Würzburg, Germany. dyakonov@physik.uni-wuerzburg.de
[d] Instituto de Ciencia Molecular, Universidad de Valencia, Catedrático José Beltrán 2, 46980 Paterna, Spain. enrique.Orti@uv.es
†Electronic Supplementary Information (ESI) available. See
DOI: 10.1039/x0xx00000x

This journal is © The Royal Society of Chemistry 20xx

Please do not adjust margins

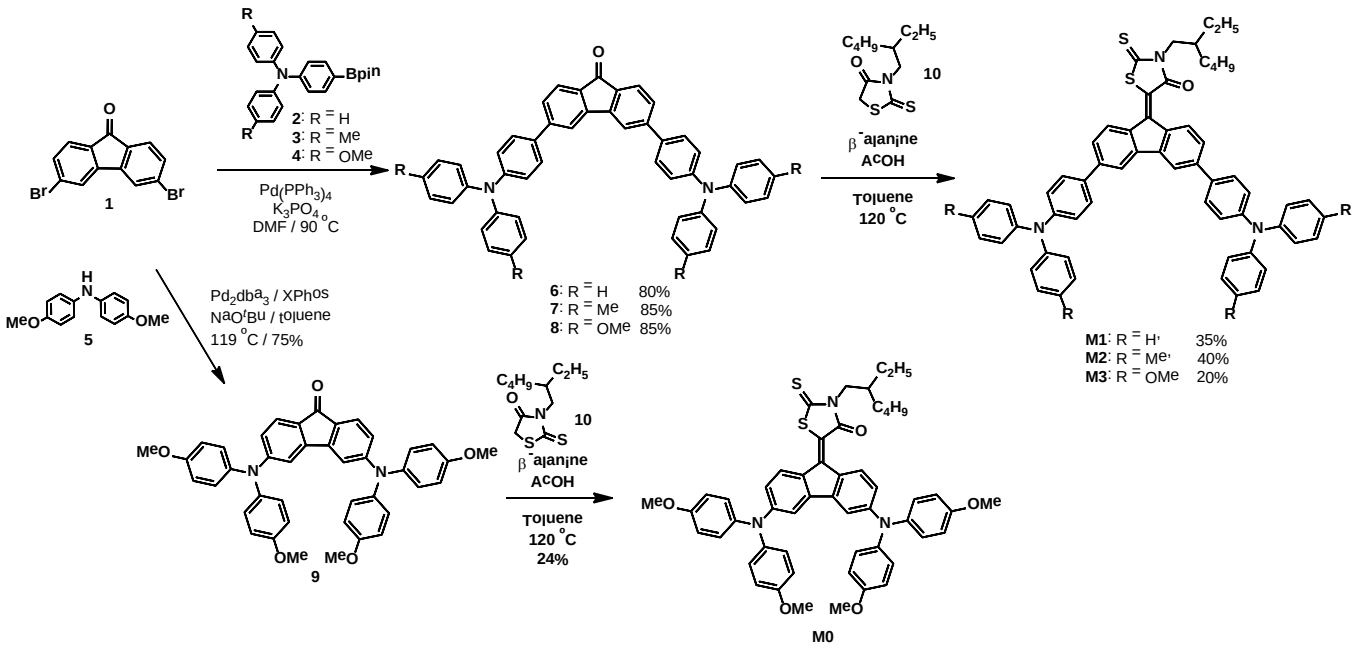

Scheme 1 Synthetic routes to dyes **M0**–**3**.

Here we present a combined experimental-computational analysis of the charge recombination rates in a novel class of small-molecule donor materials. Recent use of rhodanine acceptors (A) in dyes featuring D–A–D architecture, where different triarylamines were employed as donors (D), demonstrated the ability of small and simple organic molecules to efficiently absorb in the entire visible region.[21] Inspired by these systems we designed a new series of materials (see Fig. 1) featuring subtle modifications over the arylamine D moieties, which consisted in the use of triphenylamines (TPA) with different substituents on the *para* position of the phenyl rings (–H (**M1**), –Me (**M2**), and –OMe (**M3**)) and a diphenylamine (DPA) with –OMe substitution (**M0**). The OSCs fabricated with these materials, when employed as donors blended with the PC70BM acceptor, allowed a thorough study of the charge generation and recombination by femtosecond transient absorption (TA) spectroscopy. Modelling the TA spectra by global and target analysis, we find a significant dependence of the charge recombination rates on the electron-donating character and the steric requirements of the peripheral substituents.

Materials and Methods

Synthesis

The synthetic routes to dyes **M0–3** are shown in Scheme 1. All four dyes where straightforwardly obtained in two synthetic steps from a 3,6-dibromofluorenone (**1**) core,[22] through the sequential insertion of the donor arylamine fragment and, thereafter, the *N*-(2-ethylhexylrhodanine) acceptor.[12] Compound **M0**, bearing a diphenylamine motif as donor, was obtained by palladium C–N cross-coupling of 3,6-dibromofluorenone with bis(4-methoxyphenyl)amine, followed by Knoevenagel reaction with the rhodanine acceptor (**10**) in the presence of β-alanine and acetic acid. Similarly, derivatives **M1–3** were obtained by Suzuki-Miyaura reaction with the corresponding triarylamine boronate, followed by Knoevenagel reaction with **10**. All Knoevenagel reactions proceeded with moderate to low yields, however, starting materials were easily recovered and repeatedly used until their full conversion. Full synthetic details are available in the ESI†.

Results and discussion

Optical properties

The absorption spectra of the newly synthesised dyes are dominated by a strong (ε = 4.4 × 10^4 M^{-1} cm^{-1}) broad band covering most of the visible range (Fig. 2a and Table 1). In analogy with previous studies,[12] the lower energy band is assigned to an intramolecular charge transfer (ICT) process, as confirmed by the quantum-chemical calculations shown in the next section. As a consequence of the ICT character, this band experiences a significant bathochromic shift from 504 nm for **M1** to 541 nm for **M0**, as stronger donors are used (DPA-OMe > TPA-OMe > TPA-Me > TPA-H). It is noteworthy that DPA-OMe exerts a stronger donating effect than the TPA-OMe substituent, a fact that we attribute to the direct N–linking of the DPA units to the acceptor moiety. The onset of the optical absorption ("optical band gap") is estimated at 702 nm for **M0** and 690 nm for **M3**, while a more blue-shifted optical band gap is observed for **M2** and **M1** (652 and 640 nm, respectively). The presence of the triphenylamine moieties in **M1–3** causes a second absorption band peaking at 430 nm, which is absent in **M0**. Overall, the highest optical absorption yield for solar illumination is found with **M3** due to its extended conjugated system. The absorption of the dyes in thin films showed negligible changes with respect to the solution, which may be

 This journal is © The Royal Society of Chemistry 20xx

Please do not adjust margins

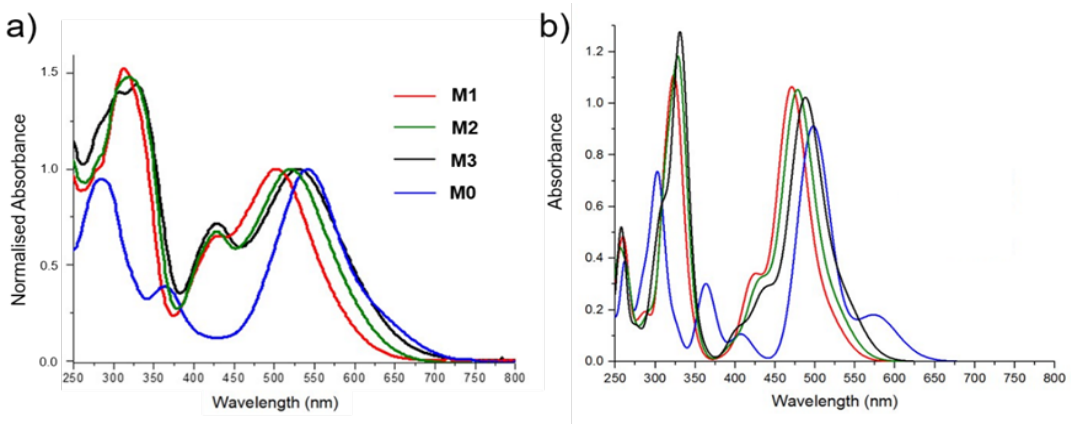

Fig. 2 a) Experimental absorption spectra of compounds **M0–3** in DCM solution. b) Theoretical simulation of the absorption spectra calculated for **M0–3** by convoluting gaussian functions centred in the positions of the TDDFT electronic excitations with a FWHM = 0.10 eV (see the ESI† for additional details).

indicative of a low tendency to form extended donor-rich domains in the blends. As explained below, this observation is not ideal for OSCs, as it tends to reduce the charge extraction efficiency. For the present study however, it is advantageous because small domains strongly reduce the importance of diffusional kinetics in the charge dynamics, allowing us to assess experimentally the elementary back transfer rate.

In order to shed light into the electronic transitions that give rise to the experimental absorption spectra, the lowest-lying singlet excited states have been computed within the time-dependent density functional theory (TDDFT) framework by using an optimally-tuned long-range corrected density functional (LC-BLYP, γ = 0.15) and the cc-pVDZ basis set (Table S3†). The simulated absorption spectra for **M0–3** compounds are shown in Fig. 2b. Note that the presence of intramolecular charge-transfer electronic transitions, owing to the D-A-D architecture of the **M0-3** compounds, advises against using standard hybrid density functionals such as the popular B3LYP (see the ESI† for a complete discussion). For the **M1–3** compounds, TDDFT calculations at the LC-BLYP(0.15)/cc-pVDZ level predict the first two $S_0 \rightarrow S_1$ and $S_0 \rightarrow S_2$ electronic transitions in the energy range of 2.15–2.41 eV and 2.49–2.64 eV, respectively, in good agreement with the position of the first absorption band experimentally recorded in the 2.25–2.48 eV range (541–504 nm, Fig. 2a and Table 1). These electronic transitions are mainly described by one-electron promotions from the HOMO and HOMO–1, localized on the donor TPA units, to the LUMO, which is centred on the fluorene-rhodanine core. They therefore imply intramolecular charge transfer from the peripheral TPA units to the acceptor central moiety. Interestingly, the $S_0 \rightarrow S_1$ and $S_0 \rightarrow S_2$ transitions are computed to decrease in energy moving from **M1** to **M2** and to **M3** (Table S3†), as the electron-donor character of the TPA-substituted moieties increases (from –H to –Me and to –OMe, respectively). For instance, the $S_0 \rightarrow S_1$ transition is found to decrease in energy from 2.41 eV (514 nm) in **M1** to 2.37 eV (522 nm) in **M2** and to 2.32 eV (534 nm) in **M3**.

These results are in good accord with the red shift experimentally recorded in the absorption spectra going from **M1** to **M3** (Fig. 2a), and with the lowering of the HOMO–LUMO gap upon increasing the electron donor character of the TPA moiety (from 2.26 eV in **M1** to 2.07 eV in **M3**; see Fig. S3†). For **M0**, the lowest-lying charge-transfer electronic transitions $S_0 \rightarrow S_1$ and $S_0 \rightarrow S_2$ are found to be well-separated at 2.16 eV (575 nm) and 2.49 eV (498 nm), respectively, being $S_0 \rightarrow S_2$ much more intense (f = 0.912) than $S_0 \rightarrow S_1$ (f = 0.178). These CT transitions should be ascribed to the experimental band recorded at 550 nm and the shoulder at 650 nm (Fig. 2a), whose respective wavelengths are slightly overestimated.

Table 1 Optical data of compounds **M0–3** in DCM solution.

Compound	λ_{max} [nm]	λ_{onset} [nm]	E_{gap}^{opt} [eV][a]	$\varepsilon(\lambda_{max})$ 10^4 [M^{-1} cm^{-1}]
M0	541	702	1.76	5.87
M1	504	640	1.93	4.38
M2	521	652	1.90	4.43
M3	531	690	1.80	4.37

[a] Calculated as $E_{gap}^{opt} = 1240/\lambda_{onset}$.

LC-BLYP(0.15)/cc-pVDZ calculations predict local excitations centred on the fluorene–rhodanine moiety in the 2.83–2.93 eV (438–423 nm) range for the **M1–3** derivatives (Table S3†), which is in good correlation with the experimental band observed at 2.90 eV (428 nm). Likewise, the analogous transition in the **M0** derivative is calculated at 3.43 eV (362 nm), matching perfectly the position of the feature experimentally recorded at 3.44 eV (360 nm). Note that this transition is better described by a DPA → fluorene charge transfer rather than a local excitation of the fluorene-rhodanine core. Finally, the intense absorption bands in the high-energy region (< 350 nm, Fig. 2b) originate from a large number of moderately intense transitions, the most important being local excitations centred on the TPA/DPA donor moieties (see, for example, state S_{11} in Table S3† for TPA-containing **M1–3** derivatives).

Electrochemical properties

The cyclic voltammograms recorded for dyes **M0–3** (Fig. S1) clearly show the ambipolar nature of these D–A–D materials. In the cathodic zone, compounds **M1–3** exhibit two reversible waves attributed to the reduction of the rhodanine acceptor. As

Please do not adjust margins

for **M0**, the molecule seems to experience three non-reversible reductions. The first reduction potential of all four compounds seems to slowly decrease from **M1** to **M3**, with a larger shift of *ca.* 100 mV for **M0**, as stronger electron donors are used in the system. Scanning the anodic zone, compounds **M1**–**3** exhibit a single reversible oxidation process related with the triphenylamine group oxidation. With the increase of donor strength from TPA-H < TPA-Me < TPA-OMe there is a noticeable 260 mV cathodic shift in the oxidation potential from **M1** (1.16 V) to **M3** (0.90 V). Compound **M0**, on the other hand, exhibits two oxidation processes (at 0.96 and 1.04 V), tentatively attributed to the sequential oxidation of the two diphenylamine groups. As shown in Table S1, a rise of the HOMO energy is observed as stronger electron-donating substituents are attached to the arylamine groups, increasing from −5.56 (**M1**) to −5.30 eV (**M3**). On the other hand, in contrast, the LUMO level shows a negligible effect of the donor strength when considering **M1**–**3**, whereas **M0** has a higher energy LUMO by around 0.1 eV.

Photovoltaic properties

We have blended **M0–3** with the standard acceptor [6,6]-phenyl C_{71} butyric acid methyl ester (PC70BM), varying the M:PC70BM blending ratio from 1:3 to 3:1. From the blends, OSC devices were produced by spin coating deploying PEDOT:PSS and Ca as electron- and hole-blocking layers, respectively (see the ESI† for details). The resulting electrical parameters are given in Table 2 for the 1:3 blends which have shown superior behaviour. The overall values for the power conversion efficiency PCE are in the range of 1.5–3.6%, which is not sufficient for commercial application. However, note that the open circuit voltages (V_{OC}), approach 1 V for **M1** and **M2**, showing the potential of this class
of materials. It is also worth mentioning the good correlation between the V_{OC} and the HOMO energy of dyads **M0**–**3**, for which the deeper the HOMO the higher the V_{OC} is. While all fill factors (FF) are relatively close together, between 33 and 40% for **M1** and **M2**, respectively, the values for the short circuit current (J_{SC}) vary over more than a factor of two, from 4.1 up to 9.5 mA/cm^2 for **M3** and **M2**, respectively. Thus, from the data in Table 2, we can conclude that under the chosen preparation conditions, all devices have similarly sub-optimal charge extraction efficiencies (reducing the FF), while significant differences prevail with respect to the efficiencies of free carrier understand whether these differences are due to different yields for exciton dissociation or for geminate charge recombination. As both processes are ultrafast, the distinction is best made in the time domain, using transient absorption spectroscopy.

Table 2 Optical and electrical characterization of compounds **M0**–**3**, blended with PC70BM. Energies are given in eV, power conversion efficiency (PCE) values in %, for the 1:3 blending ratio.

Compound	$E(S_0S_1)$	$E(S_1S_n)$	PCE,%	J_{SC}, mA/cm^2	V_{OC},V	FF,%
M0	2.25	1.2	1.5	4.6	0.88	37
M1	2.48	0.9	1.8	5.8	0.97	33
M2	2.36	1.1	3.6	9.5	0.95	40
M3	2.30	1.05	1.3	4.1	0.85	38

Transient absorption analysis

To identify elementary loss channels that could explain the electrical performance data in Table 2, we performed transient absorption (TA) spectroscopy from femtosecond to microsecond time scale. In Fig. 3a, we present femtosecond (fs) TA spectra of a film of pure **M2** after excitation with 150 fs pump pulses at 520 nm (2.5 eV) into the lowest energetic absorption band. We observe a band of formally negative TA around 2.3-2.4 eV, caused by a superposition of transient photobleach and stimulated emission bands (PB and SE, respectively).

Moreover, we observe photoinduced absorption (PA) bands (causing a positive TA signal) at about 1.0 and 2.0 eV (labelled PAS1 and PAS2, respectively). In pure donor films, it is reasonable to assign these two PA bands to optical transitions

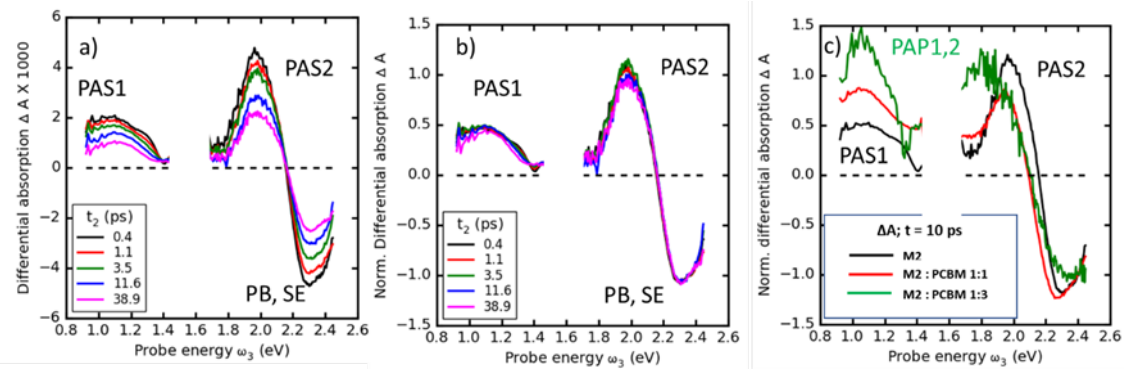

Fig. 3 (a) Femtosecond transient absorption (TA) spectra in a film of pure **M2** after pumping at 2.5 eV with 150 fs pulses. (b) Like (a), but normalized at a probe energy ω_3 = 2.4 eV. (c) Femtosecond TA spectra, normalized at 2.4 eV at a pump-probe delay t = 10 ps for a pure **M2** film and for blends with PCBM in a ratio of 1:1 and 1.3 (black, red and green curves, respectively). All films pumped at 2.5 eV with comparable pump energy.

This journal is © The Royal Society of Chemistry 20xx

Please do not adjust margins

Please do not adjust margins

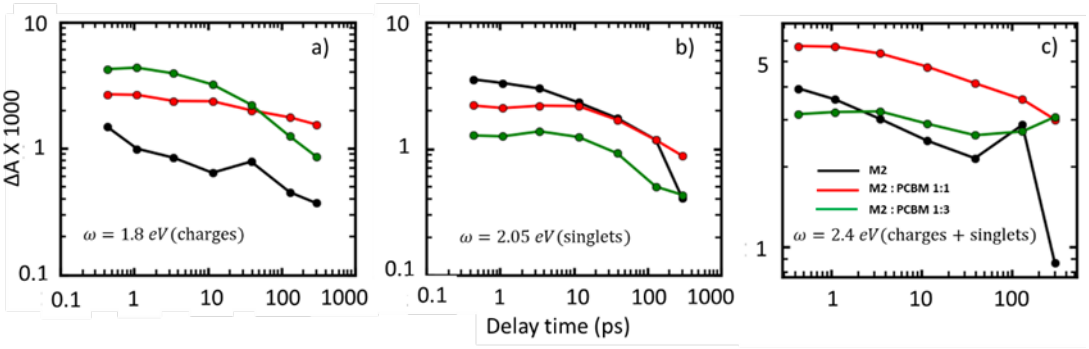

Fig. 4 TA time traces at fixed probe energies ω_3 for **M2** in pure films and blended with PCBM in 1:1 and 1:3 ratios (black, red, and green traces, respectively). (a) Probe energy ω_3 = 1.8 eV, characteristic for charged states. (b) Probe energy ω_3 = 2.05 eV, characteristic for singlet states. (c) Probe energy ω_3 = 2.4 eV, characteristic for the ground state bleach (summing up all excited states).

from the lowest excited singlet state to higher excited singlet states ($S_1 \rightarrow S_m$ and $S_1 \rightarrow S_n$, respectively) and therefore to optical probes for the dynamics of the singlet state. This assignment is confirmed by the absence of spectral evolution on a 50 ps time scale, as evidenced by normalizing the spectra of Fig.3a to the same value at a probe energy of ω_3 = 2.4 eV, see Fig.3b. In conclusion, we find that in pure **M2** the dominant photoexcitation upon resonant pumping is the singlet exciton.

In Fig. 3c, we compare TA spectra at a pump-probe delay of t = 10 ps, for pure **M2** and for its blends with PCBM in 1:1 and 1:3 ratios (black, red and green curves, respectively). In the blends, the PAS2 band is decreased with respect to the pristine film, while an additional band peaking at 1.8 eV is observed. This band is most clearly seen in the 1:3 blend (green curve); however, note that also the 1:1 blend (red curve) shows a significantly enhanced TA signal at 1.8 eV where the pure film has very little signal. Furthermore, we note that in the blends the band of positive TA in the near infrared spectral region is sharper and more centred at 1.05 eV; also, its strength with respect to the PB band increases monotonously with increasing PCBM concentration. Therefore, we assign both the sharp feature at 1.05 eV and the new band at 1.8 eV to a photoinduced absorption of the charged state of **M2** (PAP1 and PAP2, respectively). This assignment is conformed by quantum chemical calculations, yielding two photoinduced absorption bands D_{13} and D_2 with energetic offsets against the ground state absorption of −0.4 and −1.6 eV, respectively, with similar overall oscillator strengths, confirming the experimental results (see ESI, Figure S36).

In Fig. 4, we show time traces at fixed probe energies of 1.8 and 2.05 eV for **M2**:PC70BM blends (Fig. 4a and 4b, respectively). According to Fig. 3c, the TA signal at these probe energies is dominated by the charged and the singlet state, respectively. We find that all time traces, for both the charged and the singlet states, are monotonously decaying over time, irrespective of the PCBM molar fraction. As shown in Fig. 4a, the maximum polaron concentration is reached on a subpicosecond time scale for all samples, and no subsequent build-up is observed on a longer time scale. We conclude that in **M2**:PC70BM blends, charge separation is predominantly a subpicosecond process not involving exciton diffusion, which can be explained by an intimate intermixing of donors and acceptor phases, in agreement with the low aggregation tendency concluded from the similarity of the solution and thin-film UV-Vis spectra.

In Fig. 4c, we additionally show time traces recorded in the maximum of the PB band at 2.4 eV. For the pure **M2** film and its 1:1 blend, the PB dynamics roughly follow the PA dynamics, *i.e.* a decay of singlet and charged states is causing also a recovery of photobleach. This is however not the case for the 1:3 blend,

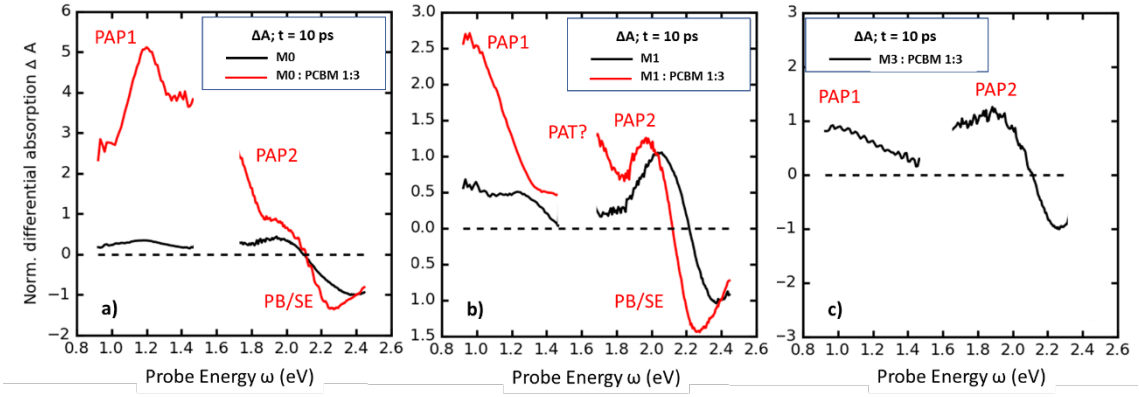

Fig. 5 TA spectra at t = 10 ps after pumping with 150 fs pulses at 2.5 eV, for **M0** (a), **M1** (b), and **M3** (c) in pure films and blended with PCBM in a ratio of 1:3. All spectra are normalized at 2.4 eV.

Please do not adjust margins

Please do not adjust margins

in which the PB is constant although the polaron bands are decaying. Since a PB is caused by a molecule not in its electronic ground state, it is an unspecific probe for the presence of excited states of any kind. Hence, we can conclude that in the **M2**:PC70BM 1:3 blend, charged states do not recombine by returning to the ground state, but by forming a different excited state. This observation points to the formation of triplet states as a consequence of charge recombination.

Owing to their similar molecular structure, all synthesized compounds show quite similar optical probes for singlet and charged states. As shown in Fig. 5, singlet states are characterized by a weak PAS1 band in the NIR spectral region and by a strong but relatively narrow PAS2 band, which is strongly superposed with the negative PB/SE bands. The charged state, which is the dominant photoexcitation when an excess of PC70BM is present, is characterized by a strong band in the near infrared and by another broad band around 1.7-1.8 eV. In all blends studied, charge separation occurs faster than 150 fs, pointing to a small domain size for donor and acceptor rich regions. This is a situation similar to polymer based OSC like un-annealed P3HT:PCBM, where the majority of the charged states are also generated on a time scale close to 60 fs.[16] Such a situation is advantageous for charge generation, since diffusive steps that may lead to exciton quenching are avoided. The down side is, however, that the concomitantly large interfacial area may give rise to enhanced charge recombination.

In Fig. 6, we compare TA time traces at the probe energies of polaron absorption (1.7 eV) and main photobleach (2.25 eV) for all blends with an M:PC70BM ratio of 1:3. All samples have been pumped at 2.4 eV at comparable pump intensities. The initial strength of TA varies from 2×10^{-3} up to 4×10^{-3}, which can be explained by different transmissions of the sample at the pump energy and by different absorption cross-sections of the charged state at 1.7 eV. For all blends, we find significant charge recombination already on the early picosecond time scale, which is the typical time scale for geminate recombination. After 300 ps, 80% of the initial polaron concentration is lost in **M1**, about 70% in **M2**, 65% in **M0** and about 50% in **M3**:PC70BM. The distinction between geminate and non-geminate charge recombination can be done by varying the pump intensity performing a target analysis (see Figure S7–10 or Table S5 on the ESI).

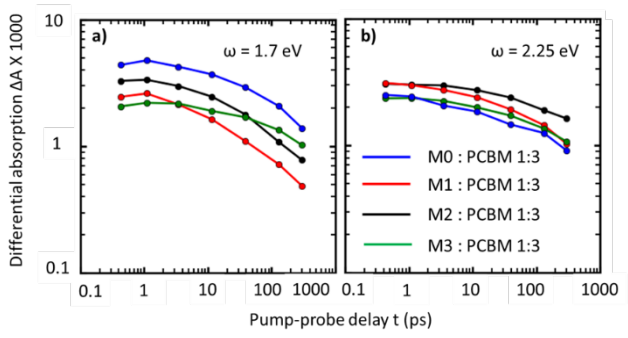

Fig. 6 TA time traces at fixed probe energies for all compounds blended with PCBM in the 1:3 ratio: (a) at a probe energy of 1.7 eV (absorption of charged states); (b) at a probe energy of 2.25 eV (ground state bleach). All samples were pumped with 150 fs pulses at 2.4 eV at comparable pump energies.

Table 3, second column, shows approximate times of 50% polaron decay due to geminate recombination, $\tau_{1/2}$, given in nanoseconds. The shortest times of geminate recombination are found in **M0** and **M3** with $\tau_{1/2}$ times of 7.5 and 6.2 ns, respectively. In **M1**, geminate recombination proceeds so slowly that we cannot give a precise value for $\tau_{1/2}$, our experimental limit being approximately 10 ns. In **M2**, finally, experimental uncertainties did not permit us to find $\tau_{1/2}$.

Table 3 Time of 50% survival for geminate recombination ($\tau_{1/2}$); "exp": from intensity dependent TA dynamics using a target analysis; "calc": by application of the Marcus-Jortner equation. For details, see SI. *) value not available due to experimental constraints. The table also shows the internal and external reorganization energies (λ_{int} and λ_{ext}, respectively) and the driving force for charge recombination, ΔG^0_{CR}, according to eq.1. All energy values given in eV.

Sample	$\tau_{1/2}$ [ns], exp	$\tau_{1/2}$ [ns], calc	λ_{int}	λ_{ext}	ΔG^0_{CR}
M0:PCBM 1:3	7.5	7	0.154	0.12	-1.66
M1:PCBM 1:3	> 10	900	0.112	0.118	-1.86
M2:PCBM 1:3	-*	190	0.106	0.114	-1.71
M3:PCBM 1:3	6.2	6	0.14	0.11	-1.59

In order to find out the reason for the different rates for geminate recombination in the compounds **M0**–**M3**, we calculated electron back transfer rates for charge recombination using the Marcus-Levich-Jortner equation in the semiclassical form which includes effects from tunnelling induced by electron-phonon coupling.[23]

$$k_{CR} = \sqrt{\frac{\pi}{\hbar^2 \lambda_s(r) k_B T}} |V(r,p)|^2 \sum_v^{\infty} \frac{e^{-S} S^v}{v!} \exp\left[\frac{-(vE_v + \lambda_s(r) + \Delta G^0_{CR}(r))^2}{4\lambda_s(r) k_B T}\right] \quad (1)$$

In eq.1, the suffix CR refers to charge recombination. The internal reorganization energy λ_v is obtained by a quantum-chemical calculation (see ESI), while E_v is the vibrational energy of an effective mode. The external reorganization energy is given by $\lambda_s(r)$, where r is the centre-to-centre distance of the oxidized donor (D) and reduced acceptor (A) excess charge densities, υ is the vibrational quantum number, V is the coupling between **D** and **A**, k_B is Boltzmann's constant, and $\Delta G^0_Y(r)$ is the Gibbs free energy change ("driving force") for charge transfer process Y, obtained by the Rehm-Weller equation:

$$\Delta G^0_Y(r) = E^D_{ox} - E^A_{red} - E_C \quad (2)$$

Where E^D_{ox} and E^A_{red} are the oxidation and the reduction potentials of donor and acceptor, respectively, as measured by cyclovoltammetry, and E_C is a correction term taking into account the different dielectric constants in the CV experiment and the solid state (For details see ESI).

The result of the calculations is shown in Table 3. We assumed an effective distance r = 1 nm between donor and acceptor and a D-A coupling constant V(r,p) = 20 meV, which is a typical value for D-A pairs.[24] With these assumptions, we

This journal is © The Royal Society of Chemistry 20xx

Please do not adjust margins

Please do not adjust margins

reproduce the fast geminate recombination times for **M0:**PC70BM and **M3:**PC70BM quite well; we furthermore find very slow geminate recombination for **M1:**PC70BM and **M2:**PC70BM, in agreement with the experimentally determined lower limit.

These drastic differences in the geminate charge recombination times can be understood by considering the calculated values for the internal and external reorganization energies (λ_{int} and λ_{ext}, respectively) and the driving force for charge recombination, ΔG_{CR}^{0}. We find that for both **M1**:PC70BM and **M2**:PC70BM, the driving forces for charge separation are high and internal reorganization energies are low. Under these conditions, charge recombination takes place far in the Marcus inverted region, explaining low recombination rates.

These results show that in a series of compounds of similar core but different substitution pattern, it is possible to qualitatively predict a trend of geminate recombination rates, by relying only on easily measurable quantities (CV, optical spectroscopy) and such that can be calculated by relatively inexpensive computational methods such as (TD)DFT. We have shown that, assuming reasonable parameters for the donor-acceptor distance, the coupling and the effective Huang-Rhys parameter, we obtain quantitative agreement between calculation and experiment. These parameters are difficult to calculate or measure; however, in a class of similar materials they can be considered as constant such that useful trends for the geminate recombination times can be obtained without the need for expensive and time-consuming methods as femtosecond spectroscopy and ab-initio quantum chemical studies.

Our method can be used to predict the optimum substituents in a specific class of donor or acceptor materials to suppress geminate charge recombination in donor-acceptor blends. Lowest geminate recombination rates are expected in the so-called 'Marcus inverted region' where the driving force (free enthalpy gain) for charge back transfer exceeds the reorganization energy, leading to a thermal activation barrier. In the quest for novel low optical bandgap donors and acceptors, providing lower driving force for recombination, special care must be taken to keep the reorganization energy as low as possible, by introducing a rigid core that avoids strong electron-phonon coupling of high frequency modes.

Conclusions

We have synthesised a series of rhodanine-based small-molecule electron donors and blended them with the PC70BM acceptor. In photovoltaic devices, we found low-to-medium power conversion efficiencies. By performing a target analysis on femtosecond spectroscopy data, we quantified the rates of geminate charge recombination. Using time-dependent density functional theory (TDDFT), we calculated the nature of the lowest energetic singlet and charged excited states as well as internal reorganization energies. Using these quantities, we were able to reproduce the measured geminate recombination times by applying the Marcus–Levich–Jortner equation. We therefore demonstrate that assuming reasonable quantities for the electronic coupling between donor and acceptor, it is possible to predict geminate recombination rates in a series of similar compounds. Our method should thus accelerate the search for high performance donor-acceptor blends based on small molecules.

Conflicts of interest

There are no conflicts to declare.

Acknowledgements

This work has been funded by the European Union (ITN "POCAONTAS", Nr 316633). We also thank the European Research Council (ERC-320441-Chirallcarbon), the Spanish Ministry of Economy and Competitiveness MINECO (projects CTQ2014-58801, CTQ2015-71154-P, CTQ2016-81911-REDT, CTQ2017-83531-R, Centro de Excelencia Severo Ochoa SEV-2016-0686 and Unidad de Excelencia María de Maeztu MDM-2015-0538), the CAM (FOTOCARBON project S2013/MIT-2841), the Generalitat Valenciana (PROMETEO/2016/135 and SEJI/2018/035) and European Feder funds (CTQ2014-58801 and CTQ2015-71154-P). J.A. is grateful to MINECO for a "Ramon-y-Cajal" fellowship (RyC-2017-23500). J.C. also acknowledges the Generalitat Valenciana for a Vali+d post-doctoral fellowship (APOSTD/2017/081).

References

1. G. Yu, J. Gao, J. C. Hummelen, F. Wudl and A. J. Heeger, *Science*, 1995, **270**, 1789-1791.
2. G. Li, V. Shrotriya, J. Huang, Y. Yao, T. Moriarty, K. Emery and Y. Yang, *Nature Materials*, 2005, **4**, 864.
3. Z. He, C. Zhong, S. Su, M. Xu, H. Wu and Y. Cao, *Nature photonics*, 2012, **6**, 591.
4. X. Guo, N. Zhou, S. J. Lou, J. Smith, D. B. Tice, J. W. Hennek, R. P. Ortiz, J. T. L. Navarrete, S. Li and J. Strzalka, *Nature Photonics*, 2013, **7**, 825.
5. J. You, L. Dou, K. Yoshimura, T. Kato, K. Ohya, T. Moriarty, K. Emery, C.-C. Chen, J. Gao and G. Li, *Nature communications*, 2013, **4**, 1446.
6. A. J. Heeger, *Advanced Materials*, 2014, **26**, 10-28.
7. R. A. Marsh, J. M. Hodgkiss, S. Albert-Seifried and R. H. Friend, *Nano letters*, 2010, **10**, 923-930.
8. Y. Liu, J. Zhao, Z. Li, C. Mu, W. Ma, H. Hu, K. Jiang, H. Lin, H. Ade and H. Yan, *Nature communications*, 2014, **5**, 5293.
9. F. Dou, E. Buchaca-Domingo, M. Sakowicz, E. Rezasoltani, T. McCarthy-Ward, M. Heeney, X. Zhang, N. Stingelin and C. Silva, *Journal of Materials Chemistry C*, 2015, **3**, 3722-3729.
10. I. Fraga Domínguez, A. Distler and L. Lüer, *Advanced Energy Materials*, 2017, **7**, 1601320.
11. O. K. Kwon, J. H. Park, D. W. Kim, S. K. Park and S. Y. Park, *Advanced materials*, 2015, **27**, 1951-1956.
12. S. Badgujar, C. E. Song, S. Oh, W. S. Shin, S.-J. Moon, J.-C. Lee, I. H. Jung and S. K. Lee, *Journal of Materials Chemistry A*, 2016, **4**, 16335-16340.

Please do not adjust margins

Please do not adjust margins

13. L. Yang, S. Zhang, C. He, J. Zhang, H. Yao, Y. Yang, Y. Zhang, W. Zhao and J. Hou, *Journal of the American Chemical Society*, 2017, **139**, 1958-1966.
14. S. Karuthedath, T. Sauermann, H.-J. Egelhaaf, R. Wannemacher, C. J. Brabec and L. Lüer, *Journal of Materials Chemistry A*, 2015, **3**, 3399-3408.
15. J. R. Ochsmann, D. Chandran, D. W. Gehrig, H. Anwar, P. K. Madathil, K. S. Lee and F. Laquai, *Macromolecular rapid communications*, 2015, **36**, 1122-1128.
16. S. M. Falke, C. A. Rozzi, D. Brida, M. Maiuri, M. Amato, E. Sommer, A. De Sio, A. Rubio, G. Cerullo and E. Molinari, *Science*, 2014, **344**, 1001-1005.
17. D. Caruso and A. Troisi, *Proceedings of the National Academy of Sciences*, 2012, **109**, 13498-13502.
18. F. Provencher, N. Bérubé, A. W. Parker, G. M. Greetham, M. Towrie, C. Hellmann, M. Côté, N. Stingelin, C. Silva and S. C. Hayes, *Nature communications*, 2014, **5**, 4288.
19. A. Isakova, S. Karuthedath, T. Arnold, J. R. Howse, P. D. Topham, D. T. Toolan, F. Laquai and L. Lüer, *Nanoscale*, 2018, **10**, 10934-10944.
20. J. Shi, A. Isakova, A. Abudulimu, M. van den Berg, O. K. Kwon, A. J. Meixner, S. Y. Park, D. Zhang, J. Gierschner and L. Lüer, *Energy Environmental Science*, 2018, **11**, 211-220.
21. R. Sandoval-Torrientes, J. Calbo, D. García-Fresnadillo, J. Santos, E. Ortí and N. J. O. C. F. Martín, *Organic Chemistry Frontiers*, 2017, **4**, 1024-1028.
22. Y. Song, W. Xu and D. Zhu, *Tetrahedron Letters*, 2010, **51**, 4894-4897.
23. T. A. Reekie, M. Sekita, L. M. Urner, S. Bauroth, L. Ruhlmann, J. P. Gisselbrecht, C. Boudon, N. Trapp, T. Clark and D. M. Guldi, *Chemistry–A European Journal*, 2017, **23**, 6357-6369.
24. Y. Yi, V. Coropceanu and J.-L. Brédas, *Journal of Materials Chemistry*, 2011, **21**, 1479-1486.

 This journal is © The Royal Society of Chemistry 20xx

Please do not adjust margins